


Cite this: *Mater. Adv.*, 2024,  
5, 5298

# Ionic liquid-based chemodosimetric probe: the selective detection and removal of bisulfite from a pure aqueous system and potential uses in biosensing†

Nishu Choudhary,<sup>ab</sup> Sanjay Yadav,<sup>ab</sup> Surjit Bhai,<sup>bc</sup> Vasavdutta Sonpal,<sup>bc</sup>  
Bishwajit Ganguly<sup>bc</sup> and Alok Ranjan Paital <sup>\*ab</sup>

The simultaneous detection and elimination of harmful substances, such as bisulfite from a pure aqueous environment using simple probe molecules that can be reused is a crucial element in promoting sustainability. In this context, most homogeneous organic probes require organic solvents with water for sensing studies, and adequate majors are not taken towards remediation of these substances. Herein, we showcase a dual-functionality approach for selectively detecting and removing bisulfite using a straightforward ionic liquid-based chemodosimetric probe that can be recycled. We utilized a hydrophilic ionic liquid for the detection phase and a hydrophobic ionic liquid for the removal phase, and this removal agent can be regenerated under basic conditions. The chemodosimetric ionic liquid-based probe, featuring an aldehyde group, engages in a nucleophilic addition reaction with bisulfite, resulting in turn-on fluorescence through ICT breakdown, as corroborated by time-dependent density functional theory (TD-DFT) studies and fluorescence lifetime studies. Notably, the probe can differentiate bisulfite from sulfite, which share similar structures and properties, with remarkable sensitivity at the nanomolar level (91 nM). This probe was also employed to detect bisulfite in living organisms and quantify it in real samples. Thus, this study demonstrates the use of a simple, cost-effective, and recyclable ionic liquid-based probe for monitoring and mitigating bisulfite in pure aqueous systems.

Received 27th February 2024,  
Accepted 27th April 2024

DOI: 10.1039/d4ma00198b

rsc.li/materials-advances

## 1. Introduction

Bisulfites ( $\text{HSO}_3^-$ ) and sulfites ( $\text{SO}_3^{2-}$ ) find common use in food preservation owing to their antimicrobial and antioxidant properties.<sup>1–3</sup> They are also the by-products of the toxic sulfur dioxide gas ( $\text{SO}_2$ ) and exist in equilibrium in aqueous systems depending on the solution pH.<sup>4,5</sup> While generally considered safe, bisulfites and sulfites at abnormal levels may lead to respiratory and gastrointestinal diseases, lung cancer, and severe allergic reactions. Recognizing their potential harm, the U.S. Food and Drug Administration (FDA) has set a

threshold limit of 10 ppm in edibles and requires their declaration on food labels.<sup>6</sup> Additionally, these substances are widely employed in industries such as leather, paper, dye, and cosmetics, leading to an increase in their concentrations in aquatic environments.<sup>7</sup> Therefore, developing effective strategies for the detection and remediation of these substances is crucial for both human health and aquatic ecosystems.<sup>8,9</sup> Among various methods, fluorescence emission-based techniques are favored because of their rapid response, non-invasiveness, sensitivity, and simplicity.<sup>10–14</sup> Numerous chemodosimetric probes<sup>15</sup> based on specific chemical reactions with bisulfite and sulfite have been reported, including nucleophilic addition reactions with electron-deficient  $\text{C}=\text{C}$  bonds<sup>16–24</sup> (Michael-type), aldehydes and ketones,<sup>25–28</sup> and deprotection of the levulinate group.<sup>29,30</sup> Apart from reactivity, hydrogen-bond mediated sensory systems have also been explored.<sup>8</sup> However, in many cases, complex synthetic steps, expensive fluorophores, poor selectivity, and limited aqueous solubility hinder their practical application in real-world and environmental samples. To address solubility issues, binary solvent systems (a mixture of water and an organic solvent) are often used. Additionally, proper

<sup>a</sup> Salt and Marine Chemicals Division, CSIR-Central Salt and Marine Chemicals Research Institute, G.B. Marg, Bhavnagar-364002, Gujarat, India.

E-mail: arpaital@csmcni.res.in

<sup>b</sup> Academy of Scientific and Innovative Research (AcSIR), Ghaziabad-201002, India

<sup>c</sup> Analytical and Environmental Science Division and Centralized Instrument Facility, CSIR-Central Salt and Marine Chemicals Research Institute, G.B. Marg, Bhavnagar-364002, India. E-mail: ganguly@csmcni.res.in

† Electronic supplementary information (ESI) available: Supplementary data containing supporting tables and figures. See DOI: <https://doi.org/10.1039/d4ma00198b>

measures for probe recycling, a critical factor in large-scale remediation applications, are often overlooked.

Given that organic fluorophores are typically either water-soluble or insoluble, achieving both sensing and removal functions in a single organic probe is challenging. However, it is possible to engineer functional ionic liquids from organic probes to achieve dual functions.<sup>31</sup> Ionic liquids were initially introduced as greener alternatives to organic solvents and later on, functionalized to derive task-specific ionic liquids for various applications.<sup>32–37</sup> They are also widely used for extraction and sensory studies. The main advantage is that it can be switched to a hydrophilic or hydrophobic ionic liquid depending on the counter anion. In our previous report, we demonstrated that both hydrophilic and hydrophobic ionic liquids can be easily derived and used for sensory and removal/extraction studies of transition metal ions.<sup>38</sup> Nevertheless, reports of such probes for the selective detection and removal of bisulfite are scarce in the literature.

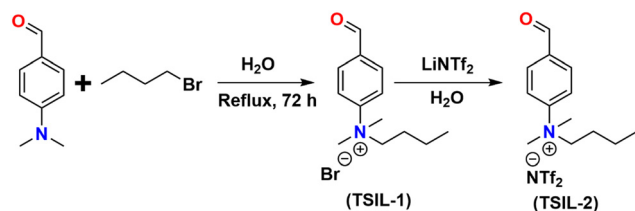
Therefore, our objective in this study was to develop an ionic liquid-based dual-functional probe, a novel approach never explored before for bisulfite. Our strategy involved creating a simple aldehyde-bearing ionic liquid species capable of undergoing nucleophilic addition reactions with bisulfite/sulfite to induce a fluorescence change. Thus, we synthesized ionic liquids from *N,N*-dimethyl benzaldehyde by simple quaternization reaction. The water-soluble hydrophilic ionic liquid (TSIL-1 with Br<sup>−</sup> anion) was employed for sensory studies, while the corresponding hydrophobic ionic liquid (TSIL-2, with NTf<sub>2</sub><sup>−</sup> anion) was used for removal studies. We also implemented a recycling process for the hydrophobic ionic liquid under basic conditions. TSIL-1 was employed for detecting bisulfite in the living organism *Artemia nauplii* and for quantifying bisulfite in sugar samples.

As far as our understanding goes, this study introduces the use of a straightforward and affordable ionic liquid for the detection of bisulfite, marking the first instance of its application in this context. Additionally, it showcases the infrequent practice of bisulfite removal.

## 2. Results and discussion

### 2.1 Synthesis and characterization

For the synthesis of a simple and cost-effective probe, *N,N*-dimethyl benzaldehyde was chosen as the starting material and converted into ionic liquids as shown in Scheme 1. Initially,



**Scheme 1** The synthetic route for hydrophilic TSIL-1 and hydrophobic TSIL-2.

*N,N*-dimethyl benzaldehyde underwent a quaternization reaction with *n*-butyl bromide in water to produce the hydrophilic ionic liquid TSIL-1. Subsequently, TSIL-1 was subjected to further reaction with LiNTf<sub>2</sub> in water to yield the hydrophobic ionic liquid TSIL-2. The ionic liquids were characterized by <sup>1</sup>H NMR, <sup>13</sup>C NMR, DSC, and mass spectrometry techniques (Fig. S1–S8, ESI<sup>†</sup>). The detailed experimental procedure is provided in the Experimental section.

### 2.2 Sensing studies

To assess the selective sensing capabilities of hydrophilic ionic liquid (TSIL-1), we conducted UV-visible and fluorescence studies both in the absence and presence of various anions within an aqueous buffer system at a pH of 7.4 (HEPES). The UV-vis spectra of TSIL-1 exhibited discernible peaks at 238 and 350 nm that corresponded to  $n \rightarrow \pi^*$  and  $\pi \rightarrow \pi^*$  transition of the electrons, respectively (Fig. 1A). It has been observed that in the presence of bisulfite, the intensity of the 350 nm peak decreases while that of the 238 nm peak is red-shifted. Such observations with all other anionic species (F<sup>−</sup>, Cl<sup>−</sup>, Br<sup>−</sup>, I<sup>−</sup>, SO<sub>4</sub><sup>2−</sup>, MoO<sub>4</sub><sup>2−</sup>, SCN<sup>−</sup>, NO<sub>3</sub><sup>−</sup>, NO<sub>2</sub><sup>−</sup>, CN<sup>−</sup>, S<sup>2−</sup>, PO<sub>4</sub><sup>3−</sup>, CO<sub>3</sub><sup>2−</sup>, H<sub>2</sub>PO<sub>4</sub><sup>−</sup>, HPO<sub>4</sub><sup>2−</sup>, SO<sub>3</sub><sup>2−</sup>, CH<sub>3</sub>COO<sup>−</sup>, and HSO<sub>3</sub><sup>−</sup>) were insignificant demonstrating the selectivity. Under similar conditions, the fluorescence spectra of TSIL-1 indicated emission maxima at 418 nm when excited at 365 nm (Fig. 1B). Upon the addition of individual anions, a remarkable surge in the fluorescence emission intensity occurred exclusively in the presence of HSO<sub>3</sub><sup>−</sup> (Fig. 1B and C). Contrarily, no significant change in emission intensity was noted with the other tested anions including sulfite. Since both sulfite and bisulfite can coexist in a balanced mixture under neutral pH conditions, two specific pH levels, namely 5.0 and 9.0, were examined for selectivity studies (Fig. 2). It has been observed that the fluorescence intensity of the probe remains constant regardless of pH, yet undergoes significant alteration upon the introduction of bisulfite, displaying pH sensitivity that remains relatively consistent over time (Fig. S9 ESI<sup>†</sup>). At pH 5.0, bisulfites are the predominant species, whereas at pH 9.0, sulfites are the dominant species. Interestingly, when examining fluorescence spectra, no noticeable changes were detected with sulfites at pH 9.0 (Fig. 2B). Conversely, a distinct increase in response, termed a “turn-on” response, was observed with bisulfite at pH 5.0 (Fig. 2A). This observation provides compelling evidence supporting the selectivity towards bisulfite in the enhancement of the emission spectra under neutral pH conditions. This difference can likely be attributed to the sulfite–aldehyde adduct’s lower stability and higher susceptibility to hydrolysis in aqueous systems compared to the bisulfite–aldehyde adduct. The enhanced stability and solubility of the bisulfite–aldehyde adduct make it the preferred option for the separation and purification of aldehydes.<sup>39</sup> This increased stability probably plays a role in the observed differentiation. The fluorescence lifetime studies were also performed in the absence and presence of bisulfite ions, where initially the probe showed a lifetime of 2.91 ns ( $\chi^2 = 1.02$ ), which increased to 3.33 ns ( $\chi^2 = 0.99$ ) confirming the selective turn-on behaviour of the probe material (Fig. S10, ESI<sup>†</sup>). To further corroborate the binding of TSIL-1 with HSO<sub>3</sub><sup>−</sup>, we conducted titration experiments, recording

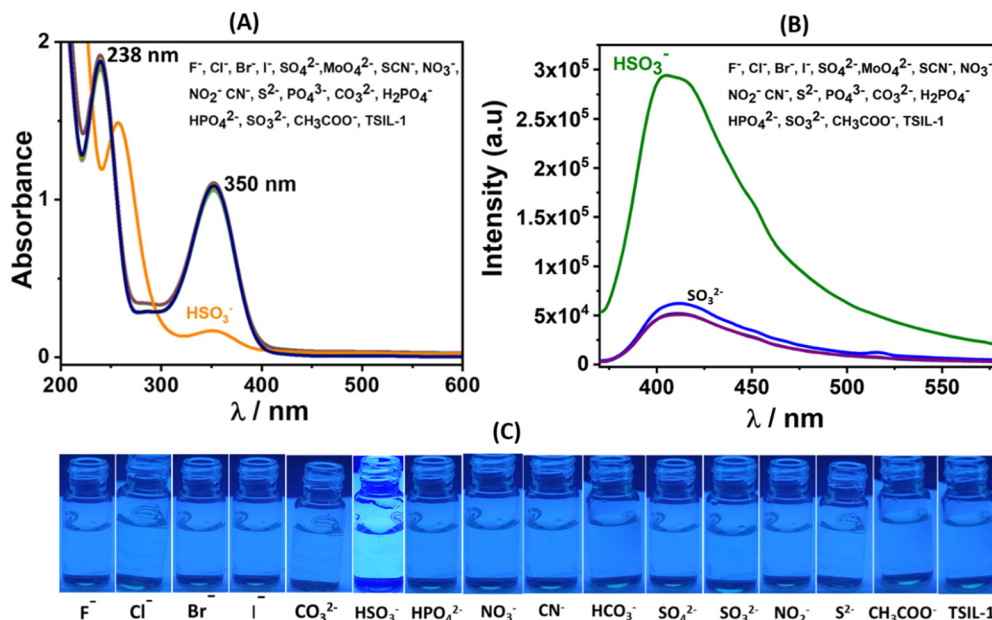


Fig. 1 (A) Absorbance spectra of **TSIL-1** with various anions at neutral pH in HEPES aqueous buffer (pH  $\sim$  7.4) (B) Emission spectra of **TSIL-1** in aqueous buffer in the presence of various anions at an excitation wavelength of 365 nm. (C) Images of the **TSIL-1** aqueous buffer solution in the presence of above anions under UV light.

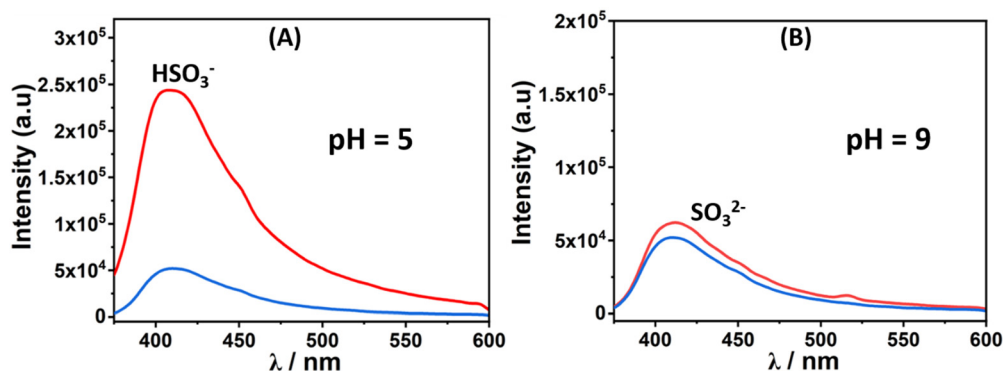


Fig. 2 Fluorescence response of **TSIL-1** with bisulfite (A) and sulfite (B) at different pH values.

emission spectra following incremental additions of  $\text{HSO}_3^-$  (Fig. 3B). The limit of detection (LOD), limit of quantification (LOQ) and linear range value ( $L-R$ ) were determined towards the bisulfite and were found to be 91 nM, 301 nM, and 0.301–25  $\mu\text{M}$ , respectively. The LOD and LOQ were calculated using  $3\sigma$  and  $10\sigma$  methods based on small incremental  $\text{HSO}_3^-$  additions (Fig. 3C). Here,  $\sigma = SD/\text{slope}$ , where  $SD$  is the standard deviation of the three blank readings and the slope is obtained from the plot of emission intensity with the concentration of the bisulfite.<sup>40</sup> The LOD value was found to be significantly lower than the prescribed limit set by the FDA.

Additionally, we determined the binding constant ( $K_b$ ) and number of binding sites ( $n$ ) by using the Scatchard equation  $[\log\{(F_0 - F)/F\} = \log K_b + n \log [\text{HSO}_3^-]]$ <sup>41</sup> from the aforementioned titration experiments, utilizing  $\text{HSO}_3^-$  saturation concentration (Fig. 3B and D). Here,  $F_0$  and  $F$  represent initial

and final fluorescence intensities, and  $[\text{HSO}_3^-]$  signifies the bisulfite concentration. The calculated binding constant ( $K_b$ ) was found to be  $\sim 4.9 \times 10^5 \text{ M}^{-1}$  with  $n$  around 0.89, which can be approximated to 1, indicating a 1:1 reaction with a good correlation factor ( $R^2 = 0.99$ ) near 1. The selective turn-on fluorescence with bisulfite in a pure aqueous system with very low detection limits makes it a suitable probe for bisulfite detection.

The chemodosimetric nature of the probe **TSIL-1** was examined by the  $^1\text{H}$  NMR spectra in  $\text{D}_2\text{O}$ . The  $^1\text{H}$  NMR of **TSIL-1** shows a signal at 9.89 ppm (Hh) for the aldehyde  $\text{HCHO}$  in  $\text{D}_2\text{O}$ , which shifted to 5.62 ppm (Hh) in the bisulfite adduct (Fig. 4). Other aromatic peaks also showed upfield shift under the influence of lowering of conjugation and electron-withdrawing influence. The proton NMR spectra of **TSIL-1** with the different stoichiometry of  $\text{NaHSO}_3$  indicate a 1:1 stoichiometric reaction



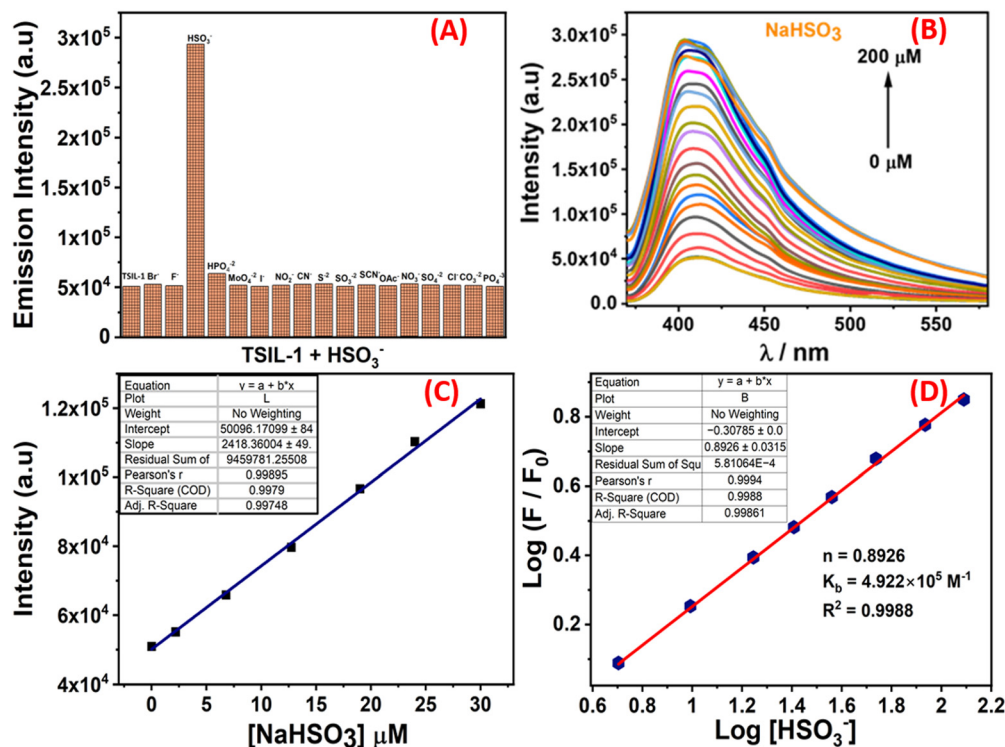


Fig. 3 (A) Relative emission intensity of **TSIL-1** with various anions. (B) Fluorescence titration spectra of **TSIL-1** with incremental addition of bisulfite at neutral pH. (C) The plot of the fluorescence intensity versus concentration of bisulfite for LOD calculation. (D) Scatchard plot from the titration experiment with bisulfite.

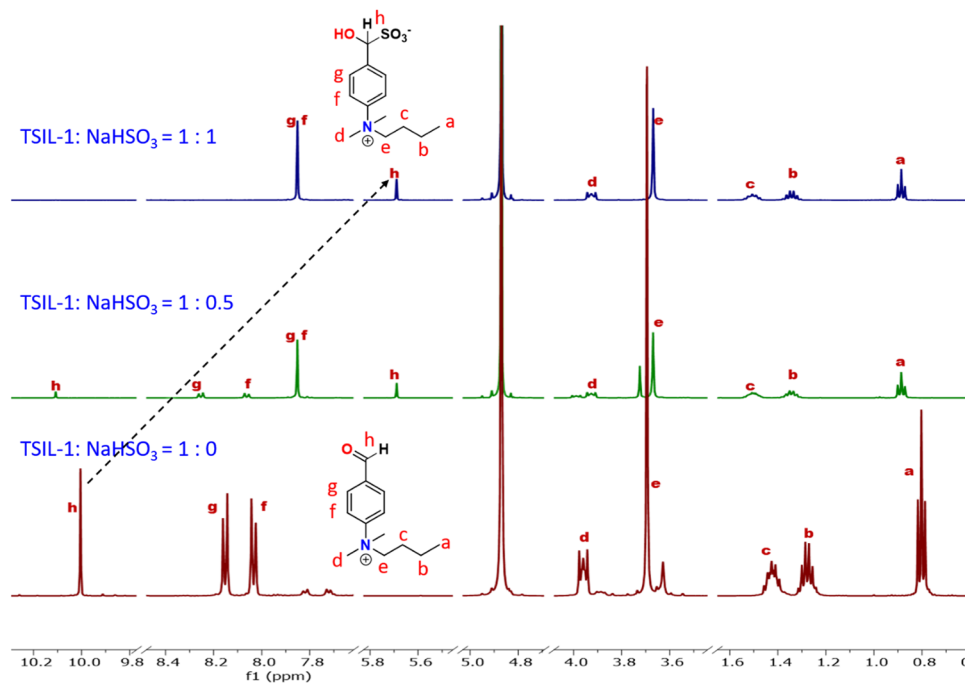


Fig. 4 <sup>1</sup>H NMR of **TSIL-1** with different stoichiometric additions of HSO<sub>3</sub><sup>-</sup> in D<sub>2</sub>O.

for completion (Fig. 4 and Fig. S11, ESI<sup>†</sup>). The mass peak for **TSIL-1** in ESI-MS is observed at  $m/z = 206.16$  for the cation

species (Fig. S3, ESI<sup>†</sup>) and with the addition of bisulfite, the corresponding **TSIL-1@HSO<sub>3</sub>** peaks are observed at 390 for



[TSIL-1@HSO<sub>3</sub> + Na<sup>+</sup>] and at 407 for [TSIL-1@HSO<sub>3</sub> + K<sup>+</sup>] (Fig. S12, ESI<sup>†</sup>).

### 2.3 DFT studies

The ground state geometries (*S*<sub>0</sub>) of **TSIL-1** and **TSIL-1@HSO<sub>3</sub>** were optimized using the B3LYP/6-31G\* level of theory (Fig. 5A and B). Further, to understand the luminescence behavior of the **TSIL-1** for the detection of bisulfite, we calculated the first excited states (*S*<sub>1</sub>) using time-dependent density functional theory (TD-DFT) at the same level of theory in the aqueous phase.<sup>42–45</sup> The TD-DFT results reveal that the orbital coefficients in **TSIL-1** is largely distributed on the anionic bromide counter ion (HOMO; −5.653 eV), whereas, the lowest unoccupied molecular orbital (LUMO; −2.633 eV) is entirely localized on the accepting group, *i.e.*, the phenyl ring (Fig. 5C and D).

Similarly, in the case of **TSIL-1@HSO<sub>3</sub>**, the HOMO (−5.580 eV) is localized on the bromide counter ion, whereas, the orbital coefficient of LUMO (−2.154 eV) resides on the phenyl ring. Such electronic transitions from anionic counter ion to the cationic part in the ionic liquid has been observed in the previous literature.<sup>46</sup> The lower energy band gap in **TSIL-1** compared to **TSIL-1@HSO<sub>3</sub>** suggests that the ICT-mediated fluorescence quenching in former case would be preferred compared to the latter case. Further, the TD-DFT results show that the fluorescence enhancement would be higher in the case of **TSIL-1@HSO<sub>3</sub>**, and corroborates the observed experimental results. Fluorescence activation through ICT is complemented by alterations in fluorescence duration, indicating an extension

in lifespan when bisulfite is present (Fig. S10, ESI<sup>†</sup>), alongside shifts in the absorption spectra (Fig. 1). Furthermore, NMR spectra verified the occurrence of nucleophilic addition reactions with bisulfite (Fig. 4).

### 2.4 Bisulfite removal and recyclability studies

Apart from bisulfite detection, the removal or remediation process is important for sustainability. However, most of the organic probes face the challenge of performing both functions simultaneously. As the **TSIL-1** is water soluble it cannot be used for the removal of bisulfite from the aqueous system. Therefore, the hydrophobic **TSIL-2** having the same cation with NTf<sub>2</sub><sup>−</sup> anion was used in the removal studies using biphasic liquid–liquid extractions in ethyl acetate as a diluent. In a standard procedure, a centrifuge tube containing 5 mL of the ionic liquid phase (**TSIL-2**) with a concentration of 0.1 mM was exposed to 10 mL of an aqueous solution containing sodium bisulfite and agitated in a mixer (Fig. 6B). The organic phase was monitored by mass, UV-vis and NMR analysis. The mass analysis of the organic phase over time shows that bisulfite adduct slowly predominates in the organic phase (Fig. S13, ESI<sup>†</sup>). The above mixture was allowed to reach equilibrium for 3–4 hours without any disturbance. Following this, some portions from the organic phase were carefully taken for UV-vis analysis (Fig. 6A). The UV-vis analysis shows similar changes as observed previously in the detection studies. Some portions of this organic phase were completely dried for NMR studies. The <sup>1</sup>H NMR spectra of this **TSIL-2@HSO<sub>3</sub>** showed complete

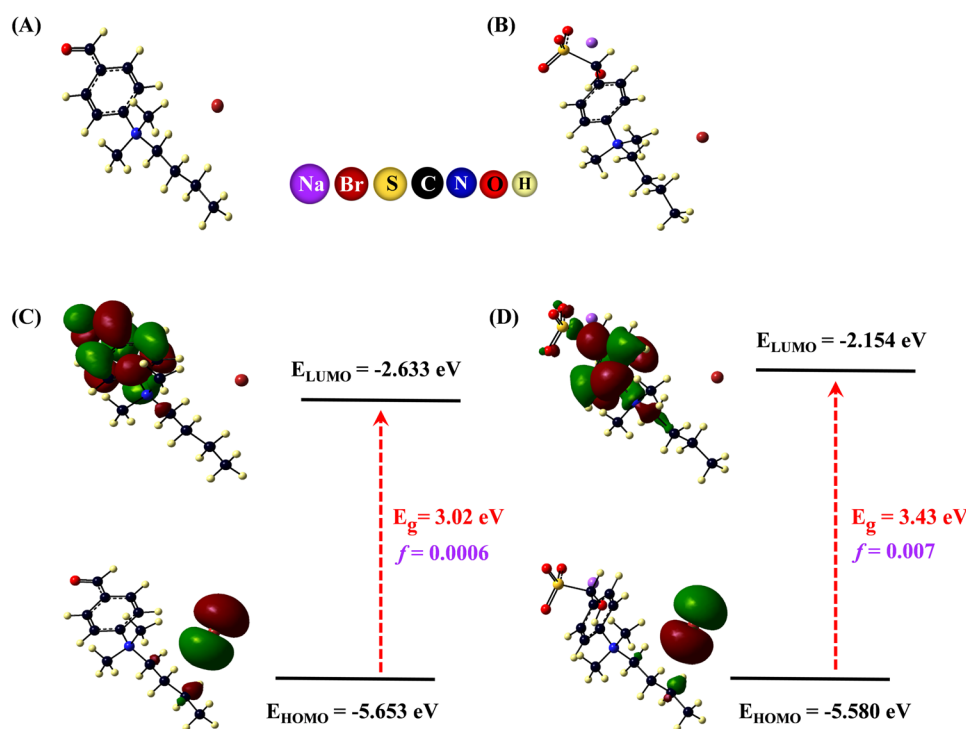
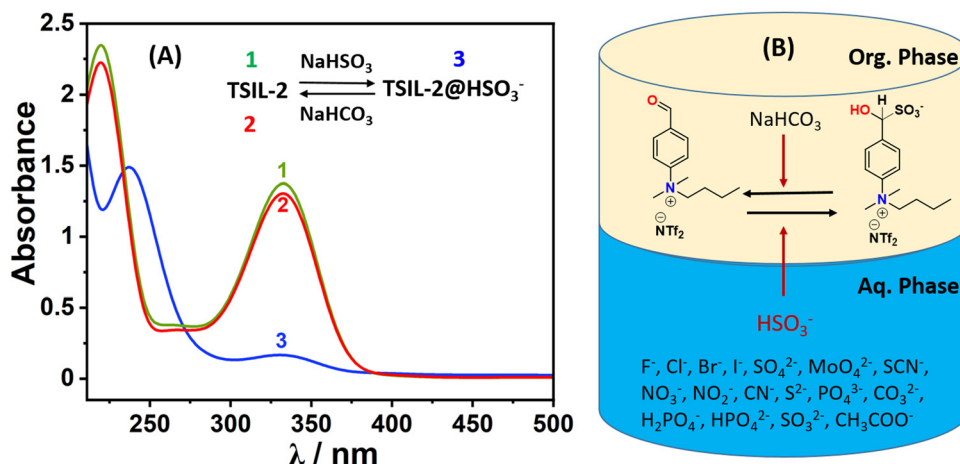


Fig. 5 (A) and (B) Optimized geometries of **TSIL-1** and the bisulfite adduct **TSIL-1@HSO<sub>3</sub>** at the B3LYP/6-31G\* level of theory in the aqueous phase. (C) and (D) HOMO and LUMO electronic distributions, energy band gap (*E*<sub>g</sub>) and oscillatory strengths (*f*) of *S*<sub>1</sub> for **TSIL-1** and **TSIL-1@HSO<sub>3</sub>** calculated using TD-DFT at the B3LYP/6-31G\* level.





**Fig. 6** (A) The UV-vis spectral monitoring of organic phase (ethyl acetate containing **TSIL-2**) during biphasic liquid-liquid extraction showing reversible binding of bisulfite (**1**: original spectrum of **TSIL-2**; **3**: spectrum after contact with  $\text{NaHSO}_3$  aq. phase; **2**: spectrum after contact with  $\text{NaHCO}_3$  aq. phase showing regeneration). (B) Pictorial representation for the removal of bisulfite from aqueous phase via liquid-liquid extraction and recyclability of **TSIL-2** with  $\text{NaHCO}_3$ .

**Table 1** The quantification of bisulfite in actual sugar samples using the **TSIL-1** probe via the fluorescence method

Samples	Proposed $\text{HSO}_3^-$ ( $\mu\text{M}$ )	Spiked $\text{HSO}_3^-$ ( $\mu\text{M}$ )	Found $\text{HSO}_3^-$ ( $\mu\text{M}$ )	Recovery (%)	RSD % ( $n = 2$ )	Titration method ( $\mu\text{M}$ )
Granulated sugar	3.49	5	9.17	108.01	2.3	8.90
		10	14.22	105.41	1.5	14.10
		15	19.16	103.62	3.48	18.94
Crystal sugar	2.83	5	7.70	98.4	2.76	7.86
		10	12.98	101.16	3.56	12.82
		15	18.13	103.42	2.87	18.10

conversion with almost 100% loading of bisulfite (Fig. S14, ESI†). Then, the aqueous phase was completely removed and the organic phase underwent a triple-washing process using miliQ water. The hydrophobic ionic liquid phase was then exposed to a basic solution (sodium bicarbonate solution with a concentration of 0.1 M). The aldehyde-bisulfite adduct is reversible under basic conditions. Therefore, this treatment caused the bisulfite anion to segregate into the aqueous phase, while the hydrophobic **TSIL-2** regenerated in the organic phase as monitored through UV-vis (Fig. 6A) and  $^1\text{H}$  NMR studies. The **TSIL-2** contained within the organic phase underwent multiple washes with deionized water and was subsequently utilized for further extraction experiments. After undergoing this recycling process for a total of three cycles, analysis of the UV-vis and NMR spectra demonstrated the presence of the original **TSIL-2**, indicating its successful retention and effective recyclability (Fig. S15, ESI†).

## 2.5 Bisulfite quantification in real samples

The real application of the probe to quantify bisulfite in actual samples was examined by fluorescence spectroscopy. Two sugar samples (crystal sugar and granulated) were investigated for the above purpose. The real sample solutions were prepared by dissolving 7 g of sugar samples separately in 10 ml of HEPES

buffer (pH 7.4) solutions to which **TSIL-1** was treated. The emission spectra were recorded for both of the samples (Fig. S16, ESI†). To know the accuracy of the method, these samples were further spiked with a known concentration of bisulfite, and the fluorescence spectra were recorded. The quantification of bisulfite was estimated from the calibration plot, which was derived from the emission titration experiments with bisulfite. The results are tabulated in Table 1, which exhibits recoveries in the range of 98 to 108% with a relative standard deviation below 5%, showing potentiality as a probe for practical applications in environmental samples.<sup>47</sup> The method's accuracy was verified through validation against a standard procedure (iodometric titration).<sup>48</sup> The comparison of the performances of the probe demonstrates various advantages over those from the literature reports (Table S1, ESI†).

## 2.6 Biosensing of bisulfite in living animal model *Artemia nauplii*

The biosensing of bisulfite in the living organism was attempted using the hydrophilic **TSIL-1** as the probe molecule through fluorescence imaging technique. In this context, brine shrimp *Artemia nauplii* was chosen as a cost-effective animal model.<sup>49</sup> The assessment of *in vivo* fluorescence imaging studies was conducted in the presence of both the **TSIL-1** and bisulfite anions, aiming to



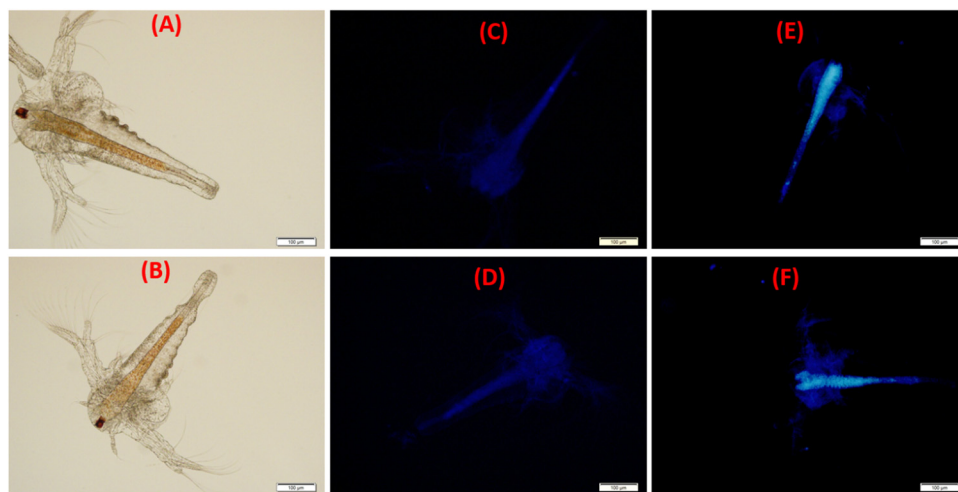


Fig. 7 (A) *Artemia nauplii* in the bright field image. (B) Bright-field image after the ingestion of TSIL-1. (C) and (D) *Artemia nauplii* after the intake of TSIL-1 in the GI tract (under the UV filter). (E) and (F) *Artemia nauplii* in the presence of bisulfite (under the UV filter).

ascertain the biosensing potential of the ionic liquid probe. For the aforementioned investigations, *Artemia* underwent treatment with the TSIL-1 solution, and fluorescence imaging was performed under the conditions with and without the bisulfite. In one particular experiment, a sample solution of TSIL-1 at a concentration of 0.1 mM was introduced into a tube containing approximately 20 organisms suspended in 10 mL of seawater. After 2 h, both bright field and fluorescence images were captured (Fig. 7A–D). The images with TSIL-1 only showed a faint blue staining of the gastrointestinal (GI) tract due to the weak fluorescent nature of TSIL-1. However, the fluorescence images after the introduction of bisulfite showed intense staining of the GI tract due to the turn-on fluorescence in the presence of bisulfite (TSIL-1@HSO<sub>3</sub><sup>−</sup>), as observed in the luminescence studies (Fig. 7E and F). These findings validate the potential biosensing application of TSIL-1 in living organisms.

## 3 Experimental section

### 3.1 Materials and methods

The reagents were procured from TCI, Sigma Aldrich, or Alfa Aesar and utilized without any additional purification. The reactions were conducted using analytical grade solvents. <sup>1</sup>H and <sup>13</sup>C NMR spectra were obtained on Bruker Avance 500 MHz and 600 MHz spectrophotometers. The EVOLUTION 201 UV-vis spectrophotometer was employed to capture UV-vis absorption spectra, while the emission spectra were recorded on the Edinburg instrument Model Xe-900 with a slit width of 1 nm. For high-resolution ESI-LCMS mass spectra, a Q-TOF Micro TM-LCMS spectrometer was used.

### 3.2 Synthesis of *N*-butyl-4-formyl-*N,N*-dimethylbenzenaminium bromide (TSIL-1)

4 g (0.0268 mmol) of 4-dimethylaminobenzaldehyde, 100 mL of water, and an excess of *n*-butyl bromide (12 mL) were combined in a two-necked round bottom flask with a magnetic stirrer.

The mixture was stirred constantly and heated to reflux for 72 hours in an oil bath of 98 °C. After completion of the reaction, the light green-colored aqueous reaction mixture was washed multiple times with chloroform and finally rotary evaporated. The result was a light brown colored viscous liquid with a 68% yield. The compound (C<sub>13</sub>H<sub>20</sub>NOBr) was characterized by <sup>1</sup>H, <sup>13</sup>C, and LC-MS: *m/z* = 206.15 (C<sub>13</sub>H<sub>20</sub>NO<sup>+</sup>), Mol. Wt. = 286.21. <sup>1</sup>H NMR (500 MHz, D<sub>2</sub>O) δ ppm/TMS values: 9.89 (s, 1H), 8.02 (d, 2H), 7.87 (d, 2H), 3.82 (t, 2H), 3.54 (s, 6H), 1.27 (m, 2H), 1.13 (m, 2H), 0.67 (t, 3H). <sup>13</sup>C NMR (500 MHz, D<sub>2</sub>O) δ ppm: 194.79, 148.98, 137.21, 132.32, 122.42, 70.10, 54.82, 25.32, 19.31, and 13.22.

### 3.3 Synthesis of *N*-butyl-4-formyl-*N,N*-dimethylbenzenaminium bis(trifluorosulfonyl) imide (TSIL-2)

To 50 mL of water in a round bottom flask, TSIL-1 (2 g, 6.98 mmol) and lithium bis (trifluoromethanesulfonamide) (2.21g, 7.68 mmol) were added and refluxed for 6 h. The water-insoluble hydrophobic ionic liquid was extracted in ethyl acetate, washed three times with distilled water, and dried to obtain a yellow viscous ionic liquid. Mol. Wt. = 486.44 g. <sup>1</sup>H NMR (CD<sub>3</sub>COCD<sub>3</sub>, 500 MHz): 10.19 (s, 1H), 8.30 (d, 2H), 8.24 (d, 2H), 4.23 (t, 2H), 3.94 (s, 6H), 1.56 (m, 2H), 1.35 (m, 2H), 0.86 (t, 3H). <sup>13</sup>C NMR (CD<sub>3</sub>COCD<sub>3</sub>, 500 MHz): δ ppm: 191.04, 148.79, 137.65, 131.28, 122.44, 119.14, 69.45, 54.47, 25.21, 19.10, and 12.82.

### 3.4 Photo-physical studies

The UV-vis and luminescence analyses of the ionic liquid probe involved using 1.430 g of TSIL-1 in an aqueous buffer (HEPES, pH ~ 7.2) medium of 500 mL. Stock solutions (0.15 mM) of various anions were prepared by dissolving the requisite amounts of sodium salts of anions (F<sup>−</sup>, Cl<sup>−</sup>, Br<sup>−</sup>, I<sup>−</sup>, SO<sub>4</sub><sup>2−</sup>, MoO<sub>4</sub><sup>2−</sup>, SCN<sup>−</sup>, NO<sub>3</sub><sup>−</sup>, NO<sub>2</sub><sup>−</sup>, CN<sup>−</sup>, S<sup>2−</sup>, PO<sub>4</sub><sup>3−</sup>, CO<sub>3</sub><sup>2−</sup>, H<sub>2</sub>PO<sub>4</sub><sup>−</sup>, HPO<sub>4</sub><sup>2−</sup>, SO<sub>3</sub><sup>2−</sup>, CH<sub>3</sub>COO<sup>−</sup>, and HSO<sub>3</sub><sup>−</sup>) in the buffer solution, each were dissolved individually using Milli-Q water.



All photophysical measurements were conducted in triplicate at room temperature. UV-vis spectra were recorded in the range of 200 to 800 nm, while fluorescence spectra were recorded in the range of 340 to 610 nm, with an excitation wavelength of 365 nm.

### 3.5 Computational methodology

The DFT optimization of all geometries was performed in the aqueous phase with a polarizable continuum model (PCM) at the B3LYP/6-31G\* level of theory.<sup>42–46</sup> Harmonic frequency calculations were conducted at the same level of theory to validate the stability of the optimized geometry, ensuring the absence of imaginary frequencies. TD-DFT method was employed to examine the excited states ( $S_0 \rightarrow S_1$ ) energies of TSIL-1 and its bisulfite adduct using the same level of theory in the aqueous phase. The HOMO and LUMO energies of both the individual ionic liquid and the bisulfite adduct were determined based on the optimized geometries. Additionally, we calculated the energy gaps, defined as the difference between the HOMO and LUMO energy levels. All these computational analyses were executed using the Gaussian 09 suite of programs.<sup>50</sup>

### 3.6 In vivo detection studies

*Artemia salina* cysts were permitted to undergo hatching overnight within a well-aerated container at room temperature, illuminated by intense visible light. The resulting hatched larvae, referred to as nauplii, were employed in the experimental procedures. In a typical experimental procedure, around 20 hatched *Artemia nauplii* were placed in 10 mL of sterile seawater. Subsequently, separate additions of TSIL-1 (each 50  $\mu$ L from a 10  $\mu$ M solution) were introduced, and the mixture was left for 2 hours. Following this incubation, a portion of the organisms was transferred onto a glass slide and observed using a BX53 OLYMPUS microscope equipped with both bright and fluorescent filters. Additionally, certain treated *Artemia nauplii* underwent incubation in a 10 mL solution of brine, containing 100  $\mu$ L of sodium bisulfite solution (10 mM). Similarly, organisms from the sample were transferred onto a glass slide and examined using the BX53 OLYMPUS microscope, utilizing both bright and fluorescent filters.

## 4 Conclusions

In summary, the primary objective of this study was to create a cost-effective probe material with dual capabilities for bisulfite sensing and removal. These functions are crucial for environmental monitoring and remediation. The approach involves the development of a probe system based on a simple ionic liquid, a rarely explored avenue for bisulfite/sulfite detection. To achieve both sensing and removal, the ionic liquid system was tailored to generate hydrophilic and hydrophobic variants. The hydrophilic ionic liquid (TSIL-1) was utilized for performing sensing studies in a pure aqueous system, while the hydrophobic counterpart

was employed for removal studies in biphasic liquid–liquid extractions. A notable advantage of this system is the absence of organic solvents in sensory studies with water. Another distinctive feature is the rare occurrence of bisulfite removal and reversibility studies in existing literature. TSIL-1 exhibits turn-on fluorescence selectively in the presence of bisulfite, with a low limit of detection (LOD) value of as low as 91 nM, well below the limit set by the World Health Organization (WHO). The turn-on fluorescence was elucidated by the breakdown of the internal charge transfer (ICT) for the chemodosimetric probe, a conclusion supported by time-dependent density functional theory (TD-DFT) studies. Furthermore, the ionic liquid probe was successfully applied for bisulfite sensing in a living organism (*Artemia nauplii*) through fluorescence imaging. Additionally, precise quantification of bisulfite in real samples was accomplished. The simplicity of the molecule's synthesis, coupled with its various advantages, positions it as a practical choice for monitoring and remediating bisulfite from aqueous systems.

## Author contributions

The collaborative effort of all authors is reflected in the creation of the manuscript, and the final version was endorsed by all the authors. N. Choudhary participated in the investigation of the work, conducted data analysis, and contributed to the writing of the original draft. S. Yadav assisted with data validation, while S. Bhai and B. Ganguly contributed to DFT studies. V. Sonpal contributed to Biosensing studies. A. R. Paital was involved in the conceptualization and reviewing/editing of the manuscript.

## Conflicts of interest

The author asserts that there are no financial or personal interests that could be perceived as influencing the research presented in this paper.

## Acknowledgements

A. R. P., B. G., N. C., S. Y., S. B., and V. S. acknowledge the Council of Scientific and Innovative Research (CSIR), Govt. of India for the financial support. N. C., S. Y., and V. S. acknowledge CSIR and AcSIR for fellowship and PhD degrees. AESD and CIF division of CSIR-CSMCRI is acknowledged to provide the analytical facility. A CSIR-CSMCRI communication no. 80/2024.

## References

- 1 R. Franco, G. Navarro and E. Martínez-Pinilla, *Antioxidants*, 2019, **8**, 542.
- 2 Y. Huang, Y. Zhang, F. Huo, J. Chao and C. Yin, *Chem. Eng. J.*, 2022, **433**, 133750.
- 3 H. Shi, R. L. Stroschne and K. Ileleji, *J. Food Prot.*, 2017, **80**, 90–95.





- 4 W. Zhang, F. Huo, Y. Yue, Y. Zhang, J. Chao, F. Cheng and C. Yin, *J. Am. Chem. Soc.*, 2020, **142**, 3262–3268.
- 5 Z. Meng, *Mutagenesis*, 2004, **19**, 465–468.
- 6 K.-F. Aguey-Zinsou, P. V. Bernhardt, U. Kappler and A. G. McEwan, *J. Am. Chem. Soc.*, 2003, **125**, 530–535.
- 7 H. Yang, Y. Du, S. Wan, G. D. Trahan, Y. Jin and W. Zhang, *Chem. Sci.*, 2015, **6**, 4049–4053.
- 8 S. Chatterjee and A. R. Paital, *Adv. Funct. Mater.*, 2018, **28**, 1704726.
- 9 H. Chen, L. Xu, W. Tuo, X. Chen, J. Huang, X. Zhang and Y. Sun, *Anal. Chem.*, 2020, **92**, 4131–4136.
- 10 L. Zeng, T. Chen, B.-Q. Chen, H.-Q. Yuan, R. Sheng and G.-M. Bao, *J. Mater. Chem. B*, 2020, **8**, 1914–1921.
- 11 M. D. Hartle and M. D. Pluth, *Chem. Soc. Rev.*, 2016, **45**, 6108–6117.
- 12 K. K.-W. Lo, *Acc. Chem. Res.*, 2020, **53**, 32–44.
- 13 J. Chan, S. C. Dodani and C. J. Chang, *Nat. Chem.*, 2012, **4**, 973–984.
- 14 H. Feng, J. Liu, A. Qaitoon, Q. Meng, Y. Sultanbawa, Z. Zhang, Z. P. Xu and R. Zhang, *TrAC, Trends Anal. Chem.*, 2021, **136**, 116199.
- 15 J. Du, M. Hu, J. Fan and X. Peng, *Chem. Soc. Rev.*, 2012, **41**, 4511.
- 16 D. Yang, X.-Y. He, X.-T. Wu, H.-N. Shi, J.-Y. Miao, B.-X. Zhao and Z.-M. Lin, *J. Mater. Chem. B*, 2020, **8**, 5722–5728.
- 17 H. Ding, G. Yuan, L. Peng, L. Zhou and Q. Lin, *J. Agric. Food Chem.*, 2020, **68**, 3670–3677.
- 18 F.-T. Liu, W.-W. Han, H. Ren, R.-N. Wang, W.-J. Yang, J.-Y. Miao, B.-X. Zhao and Z.-M. Lin, *Sens. Actuators, B*, 2023, **380**, 133305.
- 19 Z. Shang, J. Liu, Z. Hu, Q. Meng, Y. Wang, R. Zhang and Z. Zhang, *Dyes Pigm.*, 2022, **200**, 110119.
- 20 K. Zhong, Y. Yao, X. Sun, Y. Wang, L. Tang, X. Li, J. Zhang, X. Yan and J. Li, *J. Agric. Food Chem.*, 2022, **70**, 5159–5165.
- 21 Q. Zhang, X. Tang, Y. Wang, A. Song, X. Yang, D. Yin and Z. Zhang, *Spectrochim. Acta, Part A*, 2024, **305**, 123559.
- 22 A. A. Bhosle, M. Banerjee, S. Saha, S. Garg, S. Ghosh and A. Chatterjee, *Sens. Actuators, B*, 2023, **397**, 134661.
- 23 S. D. Hiremath, A. Thakuri, M. M. Joseph, A. A. Bhosle, K. K. Maiti, M. Banerjee and A. Chatterjee, *ACS Appl. Nano Mater.*, 2023, **6**, 9958–9967.
- 24 L. Jiang, T. Chen, E. Song, Y. Fan, D. Min, L. Zeng and G.-M. Bao, *Chem. Eng. J.*, 2022, **427**, 131563.
- 25 F. Cai, B. Hou, S. Zhang, H. Chen, S. Ji, X. Shen and H. Liang, *J. Mater. Chem. B*, 2019, **7**, 2493–2498.
- 26 Q. Zhang, X. Hu, X. Dai, J. Sun and F. Gao, *J. Mater. Chem. B*, 2021, **9**, 3554–3562.
- 27 H. Chen, L. Xu, W. Tuo, X. Chen, J. Huang, X. Zhang and Y. Sun, *Anal. Chem.*, 2020, **92**, 4131–4136.
- 28 C. C. Deng, Z. Y. Xu, Z. Sun, J. H. Xie, H. Q. Luo and N. B. Li, *Food Chem.*, 2023, **405**, 134961.
- 29 X. Gu, C. Liu, Y.-C. Zhu and Y.-Z. Zhu, *J. Agric. Food Chem.*, 2011, **59**, 11935–11939.
- 30 X. Ma, C. Liu, Q. Shan, G. Wei, D. Wei and Y. Du, *Sens. Actuators, B*, 2013, **188**, 1196–1200.
- 31 J. Ke, Y. Zhang, Z. Wen, S. Huang, M. Ye, Y. Tang, X. Liu and C. C. Li, *J. Mater. Chem. A*, 2023, **11**, 4428–4457.
- 32 L. Gan, J. Guo, S. Che, Q. Xiao, M. Wang, J. You and C. Wang, *Green Energy Environ.*, 2020, **5**, 195–202.
- 33 S. Che, R. Dao, W. Zhang, X. Lv, H. Li and C. Wang, *Chem. Commun.*, 2017, **53**, 3862–3865.
- 34 S. Che, L. Yin, Y. Fan, Q. Shou, C. Zhou, H. Fu and Y. She, *Sens. Actuators, B*, 2022, **360**, 131588.
- 35 S. Shaligram, P. P. Wadgaonkar and U. K. Kharul, *J. Mater. Chem. A*, 2014, **2**, 13983.
- 36 S. Chatterjee, H. Gohil, E. Suresh and A. R. Paital, *Chem. – Eur. J.*, 2015, **21**, 13943–13948.
- 37 Z. Huang, M. Yi, Y. Xu, P. Qi, Y. Liu, A. Song and J. Hao, *J. Mater. Chem. C*, 2021, **9**, 13276–13285.
- 38 H. Gohil, S. Yadav, D. Rajpurohit, G. Bhojani, S. Chatterjee and A. R. Paital, *ACS Sustainable Chem. Eng.*, 2021, **9**, 13096–13105.
- 39 D. P. Kjell, B. J. Slattery and M. J. Semo, *J. Org. Chem.*, 1999, **64**, 5722–5724.
- 40 S. Yadav, N. Choudhary and A. R. Paital, *J. Mater. Chem. A*, 2024, **12**, 202–213.
- 41 S. Chatterjee, H. Gohil, I. Raval, S. Chatterjee and A. R. Paital, *Small*, 2019, **15**, 1804749.
- 42 A. D. Becke, *J. Chem. Phys.*, 1992, **96**, 2155–2160.
- 43 C. Lee, W. Yang and R. G. Parr, *Phys. Rev. B: Condens. Matter Mater. Phys.*, 1988, **37**, 785–789.
- 44 M. M. Francel, W. J. Pietro, W. J. Hehre, J. S. Binkley, M. S. Gordon, D. J. DeFrees and J. A. Pople, *J. Chem. Phys.*, 1982, **77**, 3654–3665.
- 45 J. Tomasi, B. Mennucci and R. Cammi, *Chem. Rev.*, 2005, **105**, 2999–3094.
- 46 C. Verma and M. A. Quraishi, *e-Prime – Adv. Electr. Eng. Electron. Energy*, 2022, **2**, 100070.
- 47 S. Yadav, N. Choudhary, V. Sonpal and A. R. Paital, *Small*, 2024, **20**, 2307491.
- 48 A. Das and G. Das, *J. Photochem. Photobiol.*, 2022, **425**, 113669.
- 49 S. Yadav, N. Choudhary, V. Sonpal and A. Ranjan Paital, *Chem. Eng. J.*, 2023, **471**, 144715.
- 50 M. J. Frisch, G. W. Trucks, H. B. Schlegel, G. E. Scuseria, M. A. Robb, J. R. Cheeseman, G. Scalmani, V. Barone, B. Mennucci, G. A. Petersson, H. Nakatsuji, M. Caricato, X. Li, H. P. Hratchian, A. F. Izmaylov, J. Bloino, G. Zheng, J. L. Sonnenberg, M. Had, *et al. Gaussian 09 (revision B.1)*, Gaussian, Inc., Wallingford, CT, 2009.

